

Modification of TiO₂ with Metal Chalcogenide Nanoclusters for Hydrogen Evolution

Stephen Rhatigan, Lorenzo Niemitz, Michael Nolan

Submitted date: 02/11/2020 • Posted date: 03/11/2020

Licence: CC BY-NC-ND 4.0

Citation information: Rhatigan, Stephen; Niemitz, Lorenzo; Nolan, Michael (2020): Modification of TiO₂ with Metal Chalcogenide Nanoclusters for Hydrogen Evolution. ChemRxiv. Preprint.

<https://doi.org/10.26434/chemrxiv.13176773.v1>

Using density functional theory, corrected for on-site Coulomb interactions (DFT+U), we have investigated surface modification of TiO₂ with metal chalcogenide nanoclusters for hydrogen evolution. The nanoclusters have composition M₄X₄ (M = Sn, Zn; X = S, Se) and are adsorbed at the rutile (110) surface. The nanoclusters adsorb exothermically, with adsorption energies in the range -3.00 eV to -2.70 eV. Computed density of states (DOS) plots show that cluster-derived states extend into the band-gap of the rutile support, which indicates that modification produces a redshift in light absorption. After modification, photoexcited electrons and holes are separated onto surface and cluster sites, respectively. The free energy of H adsorption is used to assess the performance of metal chalcogenide modified TiO₂ as a catalyst for HER. Adsorption of H at nanocluster (S, Se) and surface (O) sites is considered, together with the effect of H coverage. Adsorption free energies at cluster sites in the range (-0.15 eV, 0.15 eV) are considered to be favourable for HER. The results of this analysis indicate that the sulphide modifiers are more active towards HER than the selenide modifiers and exhibit hydrogen adsorption free energies in the active range, for most coverages. Conversely, the adsorption free energies at the selenide nanoclusters are only in the active range at low H coverages. Our results indicate that surface modification with small, dispersed nanoclusters of appropriately selected materials can enhance the photocatalytic activity of TiO₂ for HER applications.

File list (2)

M4X4-modified-TiO2-HER-text.pdf (1.31 MiB)

[view on ChemRxiv](#) • [download file](#)

SuppInfo.pdf (709.77 KiB)

[view on ChemRxiv](#) • [download file](#)

Modification of TiO₂ with Metal Chalcogenide Nanoclusters for Hydrogen Evolution

Stephen Rhatigan¹, Lorenzo Niemitz¹ and Michael Nolan*^{1,2}

1: Tyndall National Institute, UCC, Lee Maltings, Dyke Parade, Cork, T12 R5CP, Ireland

2: NIBEC, Ulster University, Shore Road, Co Antrim, BT37 OQB, Northern Ireland

*Michael.nolan@tyndall.ie

Abstract

Using density functional theory, corrected for on-site Coulomb interactions (DFT+U), we have investigated surface modification of TiO₂ with metal chalcogenide nanoclusters for hydrogen evolution. The nanoclusters have composition M₄X₄ (M = Sn, Zn; X = S, Se) and are adsorbed at the rutile (110) surface. The nanoclusters adsorb exothermically, with adsorption energies in the range -3.00 eV to -2.70 eV. Computed density of states (DOS) plots show that cluster-derived states extend into the band-gap of the rutile support, which indicates that modification produces a redshift in light absorption. After modification, photoexcited electrons and holes are separated onto surface and cluster sites, respectively. The free energy of H adsorption is used to assess the performance of metal chalcogenide modified TiO₂ as a catalyst for HER. Adsorption of H at nanocluster (S, Se) and surface (O) sites is considered, together with the effect of H coverage. Adsorption free energies at cluster sites in the range (-0.15 eV, 0.15 eV) are considered to be favourable for HER. The results of this analysis indicate that the sulphide modifiers are more active towards HER than the selenide modifiers and exhibit hydrogen adsorption free energies in the active range, for most coverages. Conversely, the adsorption free energies at the selenide nanoclusters are only in the active range at low H coverages. Our results indicate that surface modification with small, dispersed nanoclusters of appropriately selected materials can enhance the photocatalytic activity of TiO₂ for HER applications.

Keywords: Photocatalysis, TiO₂, Sulphides, Selenides, Hydrogen Evolution Reaction, DFT+U

Introduction

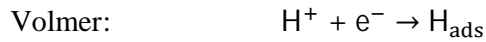
Photocatalytic water splitting, wherein solar energy is converted to chemical energy, stored in the bonds of hydrogen gas (H_2), is a promising strategy for the production and storage of clean, renewable fuel. Solar driven water splitting proceeds at the surface of a semiconductor photocatalyst material as two half reactions, mediated by photoexcited electrons and holes. The half reactions are the oxygen evolution reaction (OER) and the hydrogen evolution reaction (HER), which are oxidation and reduction reactions, respectively. Each of these reactions requires catalyst architectures that are tailored for their promotion and technologies for overall water splitting will incorporate multifunctional components for optimal efficiency.

Among the most studied photocatalytic materials is titanium dioxide (TiO_2);[1-7] TiO_2 is a cheap, non-toxic and abundant material, which is stable under photocatalytic operating conditions. However, the large band gap of TiO_2 (> 3 eV) restricts its activity to the UV range of the solar spectrum. Thus, in order to maximise the ambient solar-driven photocatalytic capacity of titania-based materials, it is necessary to modify the electronic structure to induce a redshift in light absorption. Moreover, oxide-based photocatalysts are well studied for water oxidation;[8, 9] that is, the OER half reaction. They are unsuitable for the HER without a co-catalyst. This is because H ions bind too strongly to the oxygen ions of the catalyst surface to form surface bound hydroxyls.

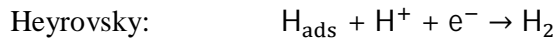
Typically, co-catalysts are employed to promote the HER and the most efficient co-catalyst materials are the platinum-group metals (PGMs).[8] PGMs are critical materials, which are rare and expensive; this limits their implementation, and thus, the viability of water splitting technologies. This provides the impetus for the considerable scientific effort devoted to the discovery of new, cheap and earth-abundant materials for efficient HER catalysis. In this endeavour, chalcogenides (sulphides, selenides and tellurides) have been demonstrated to

catalyse the HER with efficiencies approaching those of the PGMs.[8, 10] In particular, layered transition metal dichalcogenides (TMDs), containing sulphur or selenium, have garnered interest due to high HER activities.[11, 12] Through combinations of experiment and first-principles simulations, low-coordinated chalcogen sites at the edges of these layered TMDs have been identified as the active sites for HER.[13-15]

There are two proposed pathways for the two-step HER mechanism: the Volmer-Tafel reaction and the Volmer-Heyrovsky reaction.[8, 16] Here, we restrict ourselves to acidic media, as this is beneficial for the HER activity.[17, 18] The Volmer step is common to both pathways and may be described as:



In the Volmer step, an electron is transferred to a proton at an adsorption site of the catalyst surface, resulting in a surface bound H species (H_{ads}). The HER reaction is completed with desorption of a H_2 molecule, which can proceed *via* a Tafel or Heyrovsky process:



For optimal HER activity, there must be a balance between the competing adsorption and desorption steps. A widely accepted computational descriptor for this balance is the Gibbs free energy of adsorption of a H atom (ΔG_{H}) at the catalyst surface.[19] This is termed the computational hydrogen electrode model and permits a rapid comparison and assessment of different catalysts and potential active sites for H adsorption.

DFT computations of the free energy of H adsorption at low-coordinated edge sites of MoS_2 revealed that this quantity, ΔG_{H} , was close to thermoneutral (0 eV) and was comparable to that computed for Pt.[20] Conversely, ΔG_{H} for sites in the MoS_2 basal plane were endothermic and

so the basal plane is inactive for HER. Similar studies have been performed on a range of sulphides,[15, 21-23] selenides[22, 23] and phosphides[24-26] and show that ΔG_H provides a useful descriptor for screening materials and sites for their HER activity. Values for ΔG_H that are close to 0 eV are desirable, in accordance with the Sabatier principle. If the interaction is too strongly exothermic, the H ions will bind too strongly to the surface and if H adsorption is too uphill, or endothermic, no reaction will take place.[20, 24]

In this work, we examine modification of the TiO₂ rutile (110) surface with nanoclusters of composition M₄X₄ (M = Sn, Zn; X = S, Se). Surface modification in this way can be performed using atomic layer deposition,[27] incipient wetness impregnation,[28-30] or chemisorption-calcination cycles[7, 31] and permits modulation of the light absorption properties of the titania substrate, promotes separation and stability of photoexcited electrons and holes, and provides low coordinated active sites for catalytic reactions. We have studied surface-modified TiO₂ for water oxidation[32] and CO₂ activation.[33, 34] In the context of hydrogen evolution, this strategy enables us to combine the desirable properties of TiO₂ through modification with nanoclusters that display low-coordinated, active chalcogen sites, which promote the HER.

By computing the projected electronic density of states (PEDOS), we analyse the impact of modification on the energy gap and light absorption. The modification with the chalcogen nanoclusters extends the valence band maximum (VBM) to higher energies, thereby inducing a redshift in light absorption compared to unmodified TiO₂. We impose a triplet electronic state on the system to model photoexcitation and with this model, we compare the spatial separation and stability of photoexcited charges. Modification promotes the separation of electrons and holes and enhances their stability in the excited state.

Finally, we investigate the HER activity of the modified surface *via* computations of ΔG_H . To be consistent with the literature and allow for errors in computed energies within the DFT set-

up, we consider the range of $\Delta G_H = (-0.15 \text{ eV}, +0.15 \text{ eV})$ to be relevant for assessment of the potential for HER. As metal oxide surfaces easily form surface bound hydroxyls,[35] we first compute ΔG_H for H adsorbed at sites of the titania support and consider coverages that range from 1 H to enough hydrogen to saturate the available surface sites. For H adsorption at surface sites, we consider only the bridging oxygen sites (O_{br}) that have no interfacial bonds with the nanocluster modifier. For each surface H coverage, we then compute ΔG_H for H adsorption at cluster sites. In these calculations, all chalcogen sites of the modifiers are considered and the most stable configurations that we find are discussed. We find that the sulphide modifiers exhibit free energies close to thermoneutral and within our desired range at most coverages. By contrast, for the selenide modifiers, the cluster sites are active only for low surface coverages of H. We rationalise these findings on the basis of the electronic structure of the chalcogen modifiers and propose metal sulphide-modified TiO_2 as a material for hydrogen evolution.

Methodology

All calculations are performed in a periodic plane wave basis set with the VASP5.4[36, 37] code. Calculations are spin polarised and use projector augmented wave (PAW) potentials[38, 39] to describe the core-valence electron interactions. The Perdew-Wang (PW91) approximation to the exchange correlation functional is used.[40] In our earlier studies of nanocluster modified TiO_2 , [33, 41, 42] this functional provides a consistent description of these materials.[32, 43] The plane-wave energy cut-off is 400 eV; Ti is described with 4 valence electrons; Sn with 14; Zn with 12; O, S and Se with 6; and H with 1. The convergence criteria for the energy and forces are 10^{-4} eV and $0.01 \text{ eV } \text{\AA}^{-2}$, respectively. The k-points are sampled

at the Γ -point and aspherical gradient corrections are applied throughout. Gaussian smearing with $\sigma = 0.1$ eV is implemented in calculations of the density of states (DOS).

A Hubbard U correction is applied to the Ti and Zn $3d$ states with $U(\text{Ti}) = 4.5$ eV and $U(\text{Zn}) = 7.8$ eV, consistent with previous work.[44-50] These corrections are necessary in describing the partially filled d -orbital and reduced Ti^{3+} states[51, 52] and to address shortcomings in the standard GGA description of Zn electronic states.[50] An additional +U correction is applied to the O $2p$, S $3p$, and Se $4p$ states ($U = 5.5$ eV) in the photo-excited state model to describe hole localisation.[32, 41, 42, 53] We do not apply +U to anion $2p$ states for other calculations as this would make comparisons with computational studies in the literature difficult.

The bulk lattice parameters for rutile are computed as $a = b = 4.638$ Å and $c = 2.973$ Å. The model for the rutile TiO_2 substrate consists of a 12 atomic layer slab in a (2×4) expansion of the (110) surface. Periodic images are separated by a vacuum gap of 10 Å. Four metal-chalcogenide nanocluster modifiers, of compositions Sn_4S_4 , Sn_4Se_4 , Zn_4S_4 and Zn_4Se_4 are first relaxed in the gas phase (see **Figure S1** in the *Supplementary Material*) and then adsorbed in different configurations at the rutile (110) surface. The adsorption energies are computed using:

$$\Delta E_{ads} = E_{\text{NC@r110}} - E_{\text{r110}} - E_{\text{NC}} \quad (1)$$

Where $E_{\text{NC@r110}}$, E_{r110} , and E_{NC} are the energies of the composite surface, the bare surface, and the gas-phase NC, respectively. These energies can be thought of as describing the stability of the modifier on the TiO_2 substrate. Thus, a large ΔE_{ads} signifies that the modifier would only desorb at high temperatures. We adopt the notation $\text{M}_4\text{X}_4\text{-r110}$ ($\text{M} = \text{Sn}, \text{Zn}$; $\text{X} = \text{S}, \text{Se}$) for these composite surfaces.

Photoexcitation is modelled by imposing a triplet electronic state on the system. This forces an electron from the filled valence band to the empty conduction band, leaving a hole in the valence band. This computational approach has been used in previous work[32, 33, 41, 42] and

is described in detail in the *Supplementary Material*. We use this model to assess the impact of modification on the optical band gap, the stability and spatial separation of charges in the excited state.

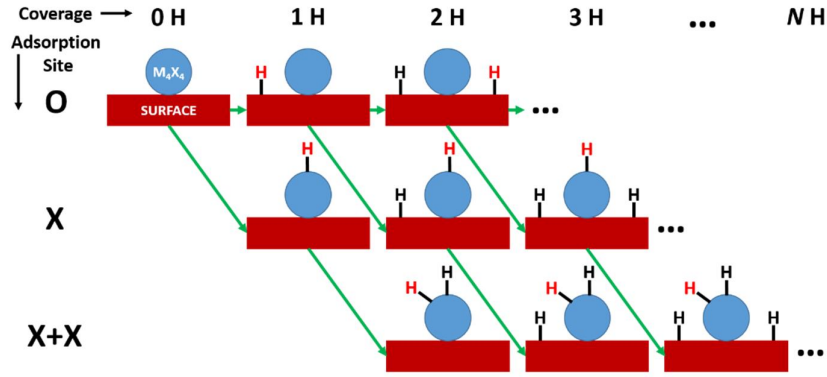


Figure 1 Schematic of the workflow for the study of hydrogen adsorption at the M_4X_4 -modified rutile (110) surface. In the first set of calculations, shown in the top row, H atoms are adsorbed at the titania surface, up to saturation of the surface (O_{br}) sites. In the second set of calculations, shown in the second row, for each coverage of H at the TiO_2 surface, one H is adsorbed at a site on the chalcogenide nanocluster. For those configurations for which the hydrogen adsorption free energy at a cluster site is in the active range, we proceed with the third set of calculations in which a second H is adsorbed at a chalcogen nanocluster site, as shown in the third row. In each image, the red H represents the current calculation.

Hydrogen adsorption is examined at both the surface and the nanocluster. We explore adsorption of H at twofold coordinated bridging O ions (O_{br}) of the rutile (110) surface and at chalcogen sites of the modifiers. We follow the workflow shown in the schematic in **Figure 1** and begin with H adsorption at O_{br} surface sites. These calculations, represented by the top row of **Figure 1**, are performed first and we identify the most stable configuration for each hydrogen coverage ranging from 0 H to saturation of the surface sites. The adsorption energy of the n^{th} H atom at the most stable surface with an existing coverage of $(n - 1)$ H atoms is computed via:

$$\Delta E_H = E_{nH@surf} - E_{(n-1)H@surf} - \frac{1}{2}(E_{H_2}) \quad (2)$$

Where $E_{nH@surf}$, $E_{(n-1)H@surf}$, and E_{H_2} are the computed energies of the surface with n H atoms adsorbed, the surface with $(n - 1)$ H atoms, and an isolated, gas phase H_2 molecule.

In the second set of calculations, represented by the second row of **Figure 1**, for each surface coverage of hydrogen, we examine hydrogen adsorption at chalcogen sites. For a surface coverage of $(n - 1)$ H, the adsorption energy of the n^{th} H atom at a cluster site is computed via:

$$\Delta E_H = E_{H@cluster} - E_{(n-1)H@surf} - \frac{1}{2}(E_{H_2}) \quad (3)$$

Where $E_{H@cluster}$ is the energy of the system with 1 H at a cluster site and $(n - 1)$ H adsorbed at surface sites. These calculations elucidate the impact of surface hydrogen coverage on the strength of interaction between H and the cluster site. For those configurations with adsorption free energies within our range, we proceed with the third set of calculations, represented by the third row in **Figure 1**, and examine adsorption of a second H atom at a cluster site to assess any trends in H coverage on the nanocluster modifier.

From the chemisorption energies (ΔE_H), we compute the free energy of adsorption using:

$$\Delta G_H = \Delta E_H + \Delta E_{ZPE} - T\Delta S_H \quad (4)$$

Where ΔE_{ZPE} is the difference in zero point energy (ZPE) between the H atom adsorbed at the surface and in the gas phase; and $T\Delta S_H$ accounts for the difference in entropy between the final and initial state. The zero point energies, for the gas phase H_2 molecule and for H adsorbed at O, S and Se sites, are derived from computations of the vibrational frequencies, according to the method prescribed in the work of Liao *et al.*[54] For adsorption, only the vibrations of the H ion and the surface/cluster site (O, S, Se) to which it is adsorbed are considered; the ZPE for the adsorption site is then subtracted from this value. As is typical in such studies, the entropic

contributions for H adsorbed at the surface are omitted, and so the value for $-\text{T}\Delta S_{\text{H}}$ is taken as half the value for molecular H_2 . Thus, the ZPE and entropic contributions to the free energy are obtained from:

$$\Delta E_{\text{ZPE}} - \text{T}\Delta S_{\text{H}} = \left(\text{ZPE}_{\text{H}^*} - \frac{1}{2} \text{ZPE}_{\text{H}_2} \right) - \left(0 - \frac{1}{2} \text{T}\Delta S_{\text{H}_2} \right) \quad (5)$$

In this way, we compute $\Delta E_{\text{ZPE}} - \text{T}\Delta S_{\text{H}}$ values of 0.35, 0.29, and 0.26 eV for H adsorbed at O, S, and Se sites, respectively and are consistent with other values used in the literature.[24, 54-56]

Results

Atomic structure

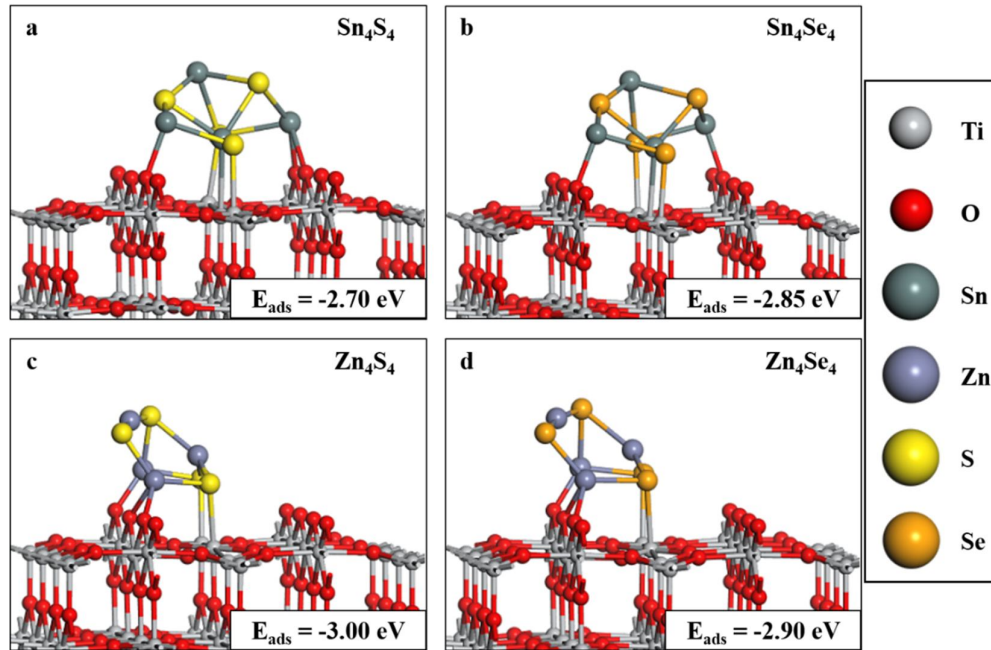


Figure 2 Relaxed geometries of (a) Sn_4S_4^- , (b) Sn_4Se_4^- , (c) Zn_4S_4^- , and (d) Zn_4Se_4^- on rutile (110). The adsorption energies of the nanoclusters at the rutile (110) surface are included in the insets. The colour scheme in the legend on the right applies to this and subsequent Figures.

The relaxed structures of the M_4X_4 -r110 are shown in **Figure 2**; the computed adsorption energies are included in the insets. The negative adsorption energies indicate that the modifier-surface interaction is favourable and the magnitudes of these energies suggest that the nanoclusters are strongly bound at the surface.[32, 33, 41, 42, 53]

For Sn_4S_4 -r110, shown in **Figure 2.a**, there are two Ti-S bonds of length 2.5 Å and three Sn-O bonds of lengths 2.2-2.4 Å. For Sn_4Se_4 -r110, in **Figure 2.b**, there are two Ti-Se bonds of lengths 2.7 and 2.8 Å and two Sn-O bonds of length 2.2 Å. For both Sn_4S_4 -r110 and Sn_4Se_4 -r110, an additional bond forms between one Sn ion and a surface Ti with a bond length of 2.9 Å.

For Zn_4S_4 -r110, shown in **Figure 2.c**, there are two Ti-S bonds of lengths 2.5 and 2.6 Å and three Zn-O bonds; one Zn-O bond is 1.9 Å and two have length 2.1 Å. For Zn_4Se_4 -r110, in **Figure 2.d**, there are two Ti-Se bonds of lengths 2.6 and 2.7 Å and three Zn-O bonds of length 1.9, 2.1 and 2.2 Å.

From these data, we can see that the Ti-S bonds are shorter than the Ti-Se bonds. This is expected as Se has a larger ionic radius than S.[8, 10] Nanocluster metal-S bonds are also shorter than metal-Se bonds, both in the gas-phase and after adsorption at the rutile TiO_2 surface. Metal-S bonds are consistently shorter by 0.12-0.16 Å, than equivalent bonds in the selenide structures. These values are in agreement with the ionic radii of S^{2-} and Se^{2-} , which are 1.84 and 1.98 Å, respectively.[57] However, despite differences in the composition of the nanocluster modifiers, the adsorption energies are similar in all cases.

Density of states

The projected electronic density of states (PEDOS) plots, computed for the M_4X_4 -r110 heterostructures, are shown in **Figure 3**. The VBM of the titania support has been set to 0 eV

and the band gap of the rutile (110) surface, from this computational set-up, is 2.20 eV. After modification, occupied cluster-derived electronic states, which are predominantly chalcogen p states, extend into the energy gap. Occupied states emerge at 1.17, 1.28, 1.26 and 1.47 eV above the titania VBM for modification with Sn_4S_4 , Sn_4Se_4 , Zn_4S_4 and Zn_4Se_4 , respectively. This is combined with an enhancement of the DOS near the VBM of the titania support due to modification. Moreover, for Sn_4X_4 modification, Sn-derived states emerge in the energy gap. These states are due to the lone pair, as has been discussed in previous work on Sn chalcogenides.[58, 59]

Thus, the modified surfaces exhibit a redshift in the energy gap, with respect to the unmodified rutile (110) surface. Moreover, modifier-derived states near the Fermi level will have important consequences for the HER activity.

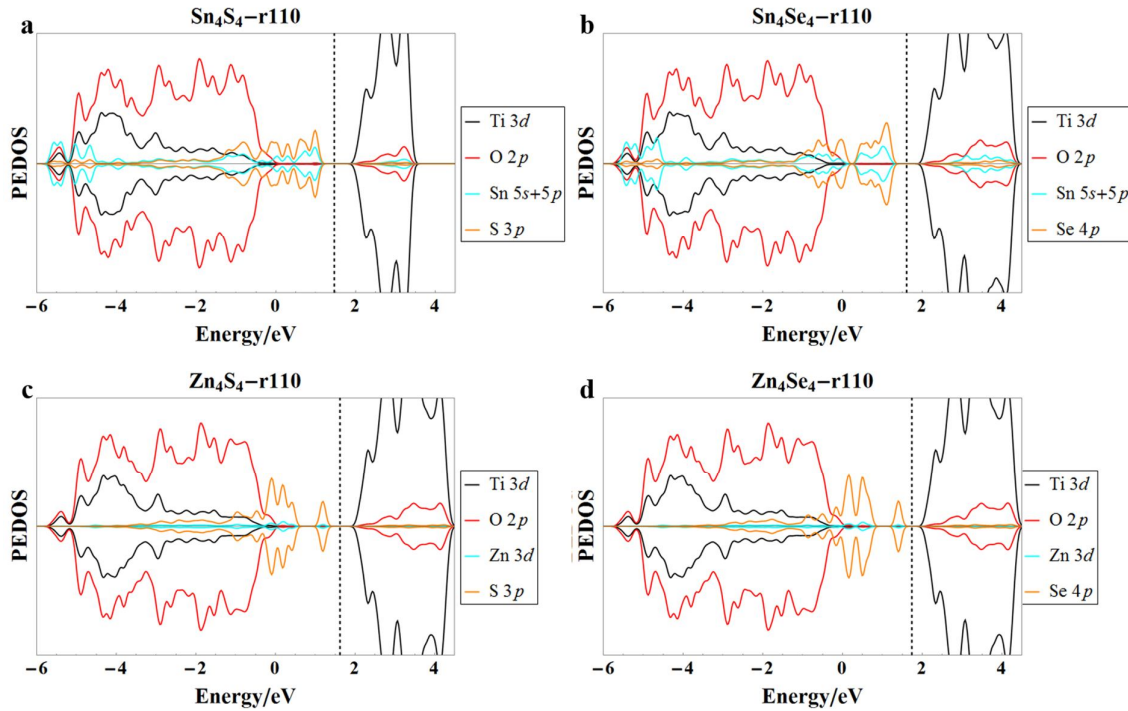


Figure 3 Density of states (DOS) plots for (a) Sn_4S_4 -, (b) Sn_4Se_4 -, (c) Zn_4S_4 -, and (d) Zn_4Se_4 -r110. The VBM of the titania support is set to 0 eV and the dashed vertical lines indicate the Fermi level. Nanocluster contributions, (M = Sn, Zn and X = S, Se), are shown ($\times 10$) for clarity.

Photoexcitation model

Table 1 Energies computed from the photoexcitation model. Vertical singlet-triplet energy difference (E^{vert}), the relaxed singlet-triplet energy difference (E^{exc}) and the relaxation energy (E^{relax}) for M_4X_4 -modified rutile (110). Values computed for the unmodified TiO_2 rutile (110) surface have been included for reference.

System	E^{vert} (eV)	E^{exc} (eV)	E^{relax} (eV)
Bare r110	2.03	1.60	0.43
Sn ₄ S ₄ -r110	1.11	0.15	0.96
Sn ₄ Se ₄ -r110	1.06	0.13	0.93
Zn ₄ S ₄ -r110	1.52	0.57	0.95
Zn ₄ Se ₄ -r110	1.25	0.13	1.13

The energies computed from the photoexcitation model are presented in **Table 1**. First, the model applied to the bare rutile (110) surface yields a vertical energy, E^{vert} , of 2.03 eV. This quantity is equivalent to the optical band gap and indicates that the underestimation of the energy gap, typical of approximate DFT methods, is present in the current computational setup. Nevertheless, this model lends itself to useful qualitative comparisons between the bare surface and the modified systems.

The values for E^{vert} indicate that modification induces a redshift in the energy gap, as was also shown in analysis of the PEDOS plots. Optical gaps of 1.11, 1.06, 1.52 and 1.25 eV are computed for the rutile (110) surface modified with Sn_4S_4 , Sn_4Se_4 , Zn_4S_4 and Zn_4Se_4 , respectively. The excitation energy, E^{exc} , is the energy difference between the singlet ground state and the fully relaxed triplet excited state. Each of the modified surfaces exhibit a reduction in this value, with respect to that computed for the bare rutile (110) surface. The computed relaxation energies, E^{rel} , are larger for the modified systems. E^{rel} represents the energy gained

by the system after structural changes and relaxation in the excited state and is a measure of the stability of electron and hole localisation. Taken together, the values shown in **Table 1** indicate that modification of rutile (110) with nanoclusters of composition M_4X_4 induces a redshift in light absorption and enhances the stability of photoexcited charges.

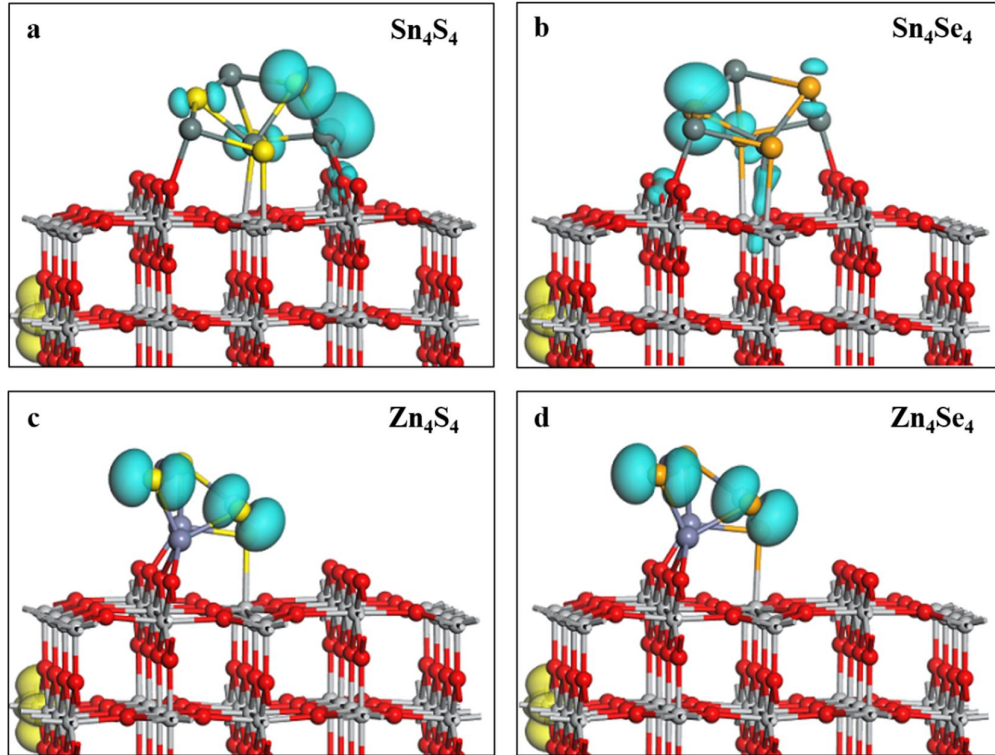


Figure 4 Excess spin density plots computed for the excited state of (a) Sn_4S_4^- , (b) Sn_4Se_4^- , (c) Zn_4S_4^- , and (d) $\text{Zn}_4\text{Se}_4\text{-r110}$, after structural relaxation. The isosurfaces enclose spin densities of up to $0.02 \text{ eV}/\text{\AA}^3$. Electrons are indicated by yellow and holes by blue.

By examining the excess spin density plots, shown in **Figure 4**, in combination with analysis of computed Bader charges and spin magnetisations, we identify at which ions the photoexcited charges localise. For each system, the electrons and holes localise at the surface and modifier, respectively, which promotes charge separation. The yellow isosurfaces show that the electrons localise at sub-surface Ti ions, resulting in a reduction from Ti^{4+} to Ti^{3+} . This is corroborated

by an increase in Bader charge from 1.3 electrons for Ti^{4+} to 1.6/1.7 electrons for Ti^{3+} and a computed spin magnetisation of $0.94 \mu_B$ for the reduced Ti^{3+} ion.

For $\text{Sn}_4\text{S}_4\text{-r110}$, the hole state localises predominantly on an S ion and a neighbouring Sn ion. For the S ion, the Bader charge decreases from 6.9 to 6.7 electrons and this ion has a spin magnetisation of $0.29 \mu_B$. For the Sn ion, the Bader charge decreases from 12.8 to 12.6 electrons, indicating some hole localisation on Sn, consistent with the DOS analysis; the spin magnetisation for this Sn ion is $0.19 \mu_B$. For $\text{Sn}_4\text{Se}_4\text{-r110}$, the hole localises on an Se ion, for which the Bader charge decreases from 6.8 to 6.4 electrons; the spin magnetisation for this ion is $0.41 \mu_B$.

For both $\text{Zn}_4\text{S}_4\text{-r110}$ and $\text{Zn}_4\text{Se}_4\text{-r110}$, the hole state is distributed over two chalcogen ions; the S ions have computed spin magnetisations of 0.27 and $0.39 \mu_B$, while for the Se ions the spin magnetisations are 0.32 and $0.35 \mu_B$. For $\text{Zn}_4\text{S}_4\text{-r110}$, the Bader charges for these S ions decrease from 6.9 and 6.8 electrons to 6.7 and 6.5 electrons, respectively. Similarly, the Bader charges for the Se ions at which the hole localises in $\text{Zn}_4\text{Se}_4\text{-r110}$ decrease from 6.8 to 6.5 electrons and from 6.6 to 6.4 electrons. In summary, each of the modified surfaces exhibit a reduction in the optical gap and an enhanced stability of excited charges, with respect to bare rutile (110). Moreover, after modification, the photoexcited electrons and holes are spatially separated; the electrons localise at subsurface Ti sites and the holes localise at chalcogen ions of the supported modifiers.

Hydrogen adsorption

Next, we examine the free energy of H adsorption at the modified surfaces and, as mentioned in the introduction, we consider that these modified materials will promote HER should they exhibit H adsorption free energies close to thermoneutral, i.e. 0 eV. For practical purposes,

values of ΔG_H between -0.15 eV and 0.15 eV are in the active range. For H adsorption at the rutile (110) surface, only the two-fold coordinated O_{br} ions are investigated. After modification, there are five such sites for Sn_4S_4 -, Zn_4S_4 - and Zn_4Se_4 -r110, and six for Sn_4Se_4 -r110; full coverage of the surface sites corresponds to five or six H atoms ($N = 5$ or 6). For each surface coverage of $n = (1 \rightarrow N)$ H, we identify the most stable configuration for the n^{th} H atom adsorbed at a surface site by computing ΔG_H relative to a surface coverage of $(n - 1)$ H atoms for each available site, using equation 2. The results of these computations are shown in the rows labelled ‘O’ for each surface in **Table 2**.

Table 2 Free energies (in eV) for H adsorption at surface sites (O) and cluster sites (S, Se) of Sn_4S_4 -, Sn_4Se_4 -, Zn_4S_4 -, and Zn_4Se_4 -r110. The data presented herein follows from the procedure described in the methodology section and summarized in the schematic in **Figure 1**. For each system and coverage, adsorption at surface sites is more favourable than adsorption at cluster sites. For adsorption of H at cluster sites, adsorption free energies in the active range are highlighted in bold.

System	Site	0H	1H	2H	3H	4H	5H	6H
Sn₄S₄-r110	O	0.00	-0.88	-0.38	-0.21	-0.46	-0.20	
	S		-0.37	-0.27	-0.09	0.22	-0.04	0.03
	S+S			-0.12	0.31	0.11	-0.12	0.27
Sn₄Se₄-r110	O	0.00	-0.68	-0.62	-0.33	-0.21	-0.14	-0.16
	Se		-0.14	0.26	0.27	0.35	0.50	0.48
	Se+Se			0.45				
Zn₄S₄-r110	O	0.00	-0.83	-0.35	-0.23	-0.24	-0.09	
	S		-0.38	-0.17	-0.11	-0.09	0.30	0.09
	S+S			0.03	0.58	0.08	0.49	0.36
Zn₄Se₄-r110	O	0.00	-0.81	-0.34	-0.31	-0.15	-0.11	
	Se		0.13	0.29	0.15	0.32	0.34	0.26
	Se+Se			0.43		0.86		

For surface coverages of between 0 and N hydrogens, we then examine hydrogen adsorption at all chalcogen sites and computed ΔG_H for the most stable chalcogen sites are presented in **Table 2**, in the rows labelled ‘X’, (X=S, Se). The adsorption free energy of the n^{th} H atom at a cluster site is calculated relative to the surface with $(n - 1)$ H at surface sites, according to equation 3. Henceforth, we distinguish between “coverage” and “surface coverage”; the former refers to the total H coverage, including adsorption sites at the nanoclusters, whereas the latter refers only to H adsorbed on O sites of the rutile (110) support.

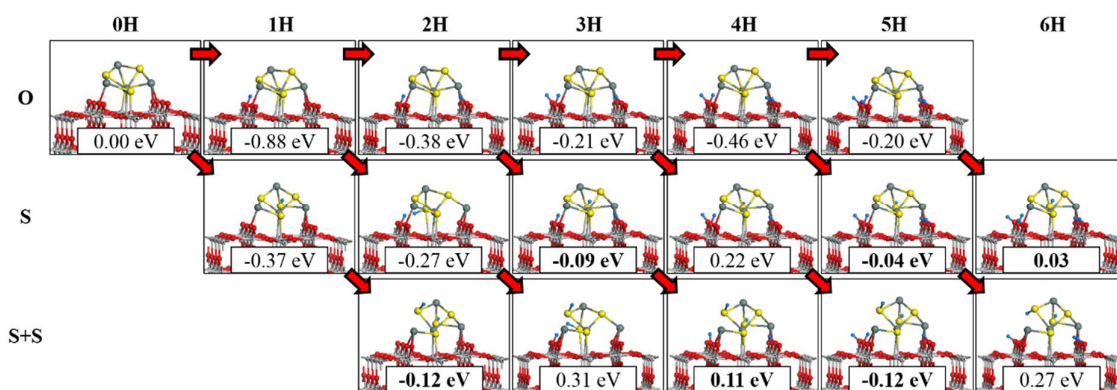


Figure 5 Adsorption configurations of H adsorbed at Sn₄S₄-r110 for coverages between one and six H atoms. The top row shows H adsorbed only at surface (O_{br}) sites, the second row shows configurations in which 1 H is adsorbed at a cluster (S) site, at each coverage. The configurations in the third row have 2 H adsorbed at S sites, for each coverage. The adsorption free energies, ΔG_H , are included in the insets and the red arrows indicate the configurations relative to which ΔG_H is computed. At all coverages, H adsorption at O_{br} sites is more favourable than adsorption at cluster sites. In this and subsequent figures, values for ΔG_H in the active range are highlighted in bold, for cluster sites.

For each modified surface, H adsorption at TiO₂ bridging oxygen sites is exothermic for all surface coverages. As the surface coverage increases, approaching full occupation of O_{br} sites, ΔG_H decreases. However, for all coverages, H adsorption at surface sites is more favourable

than adsorption at chalcogen sites. Thus, for the n^{th} H atom, ΔG_H for adsorption at a cluster site is computed relative to the system with a surface coverage of $(n - 1)$ H.

For configurations with a H atom adsorbed at a cluster site with a free energy in the active range, we also investigate ΔG_H for adsorption at a second cluster site. The results of these computations are included in the rows labelled '**X+X**' (**X**=S, Se). All adsorption configurations for the data in **Table 2** are shown in **Figure 5**, for the example of Sn₄S₄-r110, and for the remaining heterostructures, the adsorption configurations at cluster sites with energies in the active range are summarised in **Figure 6**. All adsorption configurations for the other heterostructures are shown in **Figures S3-S5** of the *Supplementary Material*.

At all coverages, the bonds formed upon H adsorption at anion sites are consistent; O-H, S-H and Se-H bonds measure in the ranges (0.97-1.00), (1.35-1.40) and (1.47-1.49) Å, respectively. For the sulphide-modified surfaces, Sn₄S₄-r110 and Zn₄S₄-r110, the first H atoms adsorb strongly at both surface and cluster sites; ΔG_H of -0.88 and -0.82 eV are computed for surface O_{br} sites and the computed ΔG_H is -0.37 and -0.34 eV for S sites. These values are quite exothermic and suggest that, at this coverage, the surface will be hydroxylated and HER is not favourable at the nanocluster as the S-H bond is too stable. However, starting from coverages of 2H, the computed ΔG_H for cluster sites are generally in the active range (-0.15 eV, 0.15 eV).

By contrast, for Sn₄Se₄-r110, only the first H adsorption free energy at a cluster site is within the active range, irrespective of the surface H coverage. Similarly, for Zn₄Se₄-r110, only two adsorption configurations are in the active range, at coverages of 1H and 3H. For higher coverages, while adsorption at O sites is favourable, adsorption at Se sites is endothermic and the free energies are outside the active range.

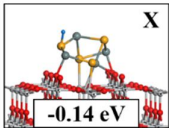
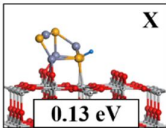
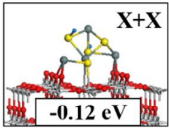
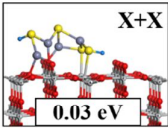
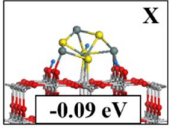
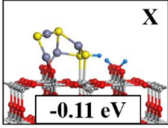
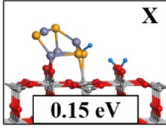
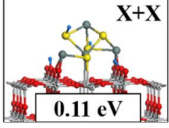
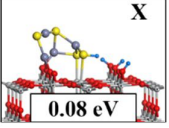
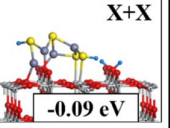
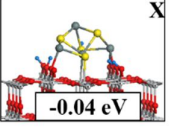
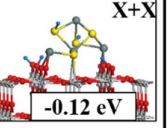
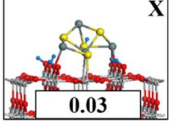
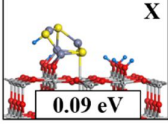
	$\text{Sn}_4\text{S}_4\text{-r110}$	$\text{Sn}_4\text{Se}_4\text{-r110}$	$\text{Zn}_4\text{S}_4\text{-r110}$	$\text{Zn}_4\text{Se}_4\text{-r110}$
1H		 X -0.14 eV		 X 0.13 eV
2H	 X+X -0.12 eV		 X+X 0.03 eV	
3H	 X -0.09 eV		 X -0.11 eV	 X 0.15 eV
4H	 X+X 0.11 eV		 X 0.08 eV  X+X -0.09 eV	
5H	 X -0.04 eV  X+X -0.12 eV			
6H	 X 0.03		 X 0.09 eV	

Figure 6 H adsorption configurations with free energies in the range (-0.15 eV, +0.15 eV), for adsorption at cluster sites of $\text{Sn}_4\text{S}_4\text{-}$, $\text{Sn}_4\text{Se}_4\text{-}$, $\text{Zn}_4\text{S}_4\text{-}$, and $\text{Zn}_4\text{Se}_4\text{-r110}$. The total H coverages are shown on the left hand side. “X” = adsorption of a single H at a chalcogen site of the cluster; “X+X” = adsorption of two H at chalcogen sites of the cluster.

In summary, the data presented in **Table 2** indicate that the sulphide-modified surfaces will be more active in HER, with respect to the selenide-modified surfaces. In general, H adsorption at S sites is more favourable than adsorption at Se sites; adsorption at Se sites is generally highly endothermic. This result is in agreement with a recent study on the stabilisation of hydrogen adsorption on Chevrel-Phase Mo_6X_8 (X=S, Se, Te) electrocatalysts.[60] Through a combination of experiment and computation, the authors reported that H adsorption strength increased with the electronegativity of the chalcogen (S = 2.58; Se = 2.55).[61] This result manifests in the electronic structure as a lower *p*-band centre. The *p*-band centre is defined as:

$$X \text{ } p\text{-band centre} = \frac{\int_{-\infty}^{\infty} E \cdot D_{Xp}(E) dE}{\int_{-\infty}^{\infty} D_{Xp}(E) dE} - E_F \quad (6)$$

This quantity can be extrapolated from the computed PEDOS and values of -2.08, -1.70, -2.22 and -1.95 eV were computed for the chalcogen species of Sn₄S₄-, Sn₄Se₄-, Zn₄S₄- and Zn₄Se₄-r110, respectively. The lower *p*-band centres for the sulphide-modified systems reflect the stronger hydrogen adsorption at cluster sites of these composite surfaces. Finally, hydroxylation of the rutile support, beyond a surface coverage of 1 H, does not qualitatively affect the strength of adsorption of H at cluster sites.

For each of the H adsorption configurations at cluster sites with ΔG_H in the range (-0.15 eV, 0.15 eV), highlighted in bold in **Table 2**, we examine the subsequent Heyrovsky step in which a H atom interactions with H bound at S or Se of the nanocluster. This results in the formation and desorption of a H₂ molecule in a process which amounts to the reverse of H adsorption; thus, the free energy corrections, $\Delta E_{ZPE} - T\Delta S_H$, are the negative of those computed for H adsorption, i.e. -0.29 eV and -0.26 eV for desorption from S and Se, respectively. For Sn₄S₄-r110, of the six adsorption configurations with ΔG_H in the active range, the desorption free energies are in the range (-0.19 eV, +0.20 eV). For the four active configurations on Zn₄S₄-r110, the desorption energies are in the range (-0.35 eV, 0.09 eV). The free energies are 0.43 eV for desorption from Sn₄Se₄- and 0.01 and -0.19 eV for desorption from Zn₄Se₄-r110. This suggests that formation of H₂ through the Heyrovsky step should be favourable on metal sulphide modified TiO₂.

Conclusions

Metal chalcogenides have emerged as promising candidates for HER catalysis. Extensive experimental and computational studies of TMDs have revealed that low-coordinated

chalcogen sites are active sites for HER. This is attributed to the near optimal adsorption free energy of H at chalcogen sites.

In this work, we have examined, *via* DFT+U computations, the surface modification of TiO₂ rutile (110) with nanoclusters of composition M₄X₄ (M = Sn, Zn; X = S, Se). Surface modification strategies aim to combine the desirable properties of the substrate (TiO₂) with those of the nanocluster modifiers. In this instance, the M₄X₄ modifiers provide low-coordinated chalcogen sites, which we have investigated for their HER activity *via* computations of the free energy of H adsorption.

Our results indicate that the M₄X₄ modifiers bind to the rutile surface with the formation of interfacial M-O and Ti-X bonds. The modification induces a red shift in light absorption due to the emergence of occupied, nanocluster-derived (predominantly chalcogen 2*p*) states in the titania energy gap. In addition, modification with M₄X₄ nanoclusters promotes the spatial separation of photoexcited charges and enhances their stability in the excited state.

Analysis of the free energies of H adsorption, ΔG_H , reveals that the sulphide modifiers exhibit values close to thermoneutral, (-0.15 eV, +0.15 eV), for most H coverages, whereas this is only true for the selenide modifiers at low coverages. This is a widely accepted descriptor for HER activity and suggests that sulphide-modification will promote the HER to a greater extent than selenide modification. In general, H binding at sulphur sites is more favourable than at selenium sites; we attribute this to the higher electronegativity of S, with respect to Se. This effect is manifested in the computed *p*-band centres of the modified systems – the sulphide-modified systems exhibit lower *p*-band centres than the selenide-modified systems.

In conclusion, modification of titania with dispersed metal chalcogenide nanoclusters has the potential to enhance the HER activity of the titania support. Careful analysis is required to elucidate the impact of modification on the properties which govern the photocatalytic HER

activity. However, rational selection of the composition of the modifiers, in combination with first principles computations of appropriate material descriptors can facilitate high-throughput screening of candidate materials.

Acknowledgements

We acknowledge support from Science Foundation Ireland through the US-Ireland R&D Partnership program, Grant number SFI/US/14/E2915 and the ERA.Net for Materials Research and Innovation (M-ERA.Net 2), Horizon 2020 grant agreement number 685451, SFI Grant Number SFI/16/M-ERA/3418 (RATOCAT). We acknowledge access to SFI funded computing resources at Tyndall Institute and the SFI/HEA funded Irish Centre for High End Computing. We are grateful for support from the COST Action CM1104 “Reducible Metal Oxides, Structure and Function”

Conflicts of interest

None

References

- [1] A. Fujishima, X. Zhang, D.A. Tryk, TiO₂ photocatalysis and related surface phenomena, *Surface Science Reports*, 63 (2008) 515-582.
- [2] M. Ni, M.K.H. Leung, D.Y.C. Leung, K. Sumathy, A review and recent developments in photocatalytic water-splitting using TiO₂ for hydrogen production, *Renewable and Sustainable Energy Reviews*, 11 (2007) 401-425.
- [3] N.M. Dimitrijevic, B.K. Vijayan, O.G. Poluektov, T. Rajh, K.A. Gray, H. He, P. Zapol, Role of Water and Carbonates in Photocatalytic Transformation of CO₂ to CH₄ on Titania, *Journal of the American Chemical Society*, 133 (2011) 3964-3971.
- [4] S.N. Habisreutinger, L. Schmidt-Mende, J.K. Stolarczyk, Photocatalytic Reduction of CO₂ on TiO₂ and Other Semiconductors, *Angewandte Chemie International Edition*, 52 (2013) 7372-7408.

- [5] M. Pelaez, N.T. Nolan, S.C. Pillai, M.K. Seery, P. Falaras, A.G. Kontos, P.S.M. Dunlop, J.W.J. Hamilton, J.A. Byrne, K. O'Shea, M.H. Entezari, D.D. Dionysiou, A review on the visible light active titanium dioxide photocatalysts for environmental applications, *Applied Catalysis B: Environmental*, 125 (2012) 331-349.
- [6] V. Etacheri, C. Di Valentin, J. Schneider, D. Bahnemann, S.C. Pillai, Visible-light activation of TiO₂ photocatalysts: Advances in theory and experiments, *Journal of Photochemistry and Photobiology C: Photochemistry Reviews*, 25 (2015) 1-29.
- [7] H. Tada, Q. Jin, A. Iwaszuk, M. Nolan, Molecular-scale transition metal oxide nanocluster surface-modified titanium dioxide as solar-activated environmental catalysts, *The Journal of Physical Chemistry C*, 118 (2014) 12077-12086.
- [8] S. Rhatigan, M.C. Michel, M. Nolan, Hydrogen evolution on non-metal oxide catalysts, *Journal of Physics: Energy*, (2020).
- [9] Z.-F. Huang, J. Wang, Y. Peng, C.-Y. Jung, A. Fisher, X. Wang, Design of Efficient Bifunctional Oxygen Reduction/Evolution Electrocatalyst: Recent Advances and Perspectives, *Advanced Energy Materials*, 7 (2017) 1700544.
- [10] X. Zou, Y. Zhang, Noble metal-free hydrogen evolution catalysts for water splitting, *Chemical Society Reviews*, 44 (2015) 5148-5180.
- [11] X. Huang, Z. Zeng, H. Zhang, Metal dichalcogenide nanosheets: preparation, properties and applications, *Chemical Society Reviews*, 42 (2013) 1934-1946.
- [12] J. McAllister, N.A.G. Bandeira, J.C. McGlynn, A.Y. Ganin, Y.-F. Song, C. Bo, H.N. Miras, Tuning and mechanistic insights of metal chalcogenide molecular catalysts for the hydrogen-evolution reaction, *Nature Communications*, 10 (2019) 370.
- [13] M.V. Bollinger, K.W. Jacobsen, J.K. Nørskov, Atomic and electronic structure of MoS₂ nanoparticles, *Phys. Rev. B*, 67 (2003) 085410.
- [14] J.V. Lauritsen, M.V. Bollinger, E. Lægsgaard, K.W. Jacobsen, J.K. Nørskov, B.S. Clausen, H. Topsøe, F. Besenbacher, Atomic-scale insight into structure and morphology changes of MoS₂ nanoclusters in hydrotreating catalysts, *Journal of Catalysis*, 221 (2004) 510-522.
- [15] T.F. Jaramillo, K.P. Jørgensen, J. Bonde, J.H. Nielsen, S. Hørch, I. Chorkendorff, Identification of Active Edge Sites for Electrochemical H₂ Evolution from MoS₂ Nanocatalysts, *Science*, 317 (2007) 100-102.
- [16] P. Xiao, W. Chen, X. Wang, A Review of Phosphide-Based Materials for Electrocatalytic Hydrogen Evolution, *Advanced Energy Materials*, 5 (2015) 1500985.
- [17] C. Hu, L. Zhang, J. Gong, Recent progress made in the mechanism comprehension and design of electrocatalysts for alkaline water splitting, *Energy & Environmental Science*, 12 (2019) 2620-2645.
- [18] P.C.K. Vesborg, B. Seger, I. Chorkendorff, Recent Development in Hydrogen Evolution Reaction Catalysts and Their Practical Implementation, *The Journal of Physical Chemistry Letters*, 6 (2015) 951-957.
- [19] N. Dubouis, A. Grimaud, The hydrogen evolution reaction: from material to interfacial descriptors, *Chemical Science*, 10 (2019) 9165-9181.
- [20] B. Hinnemann, P.G. Moses, J. Bonde, K.P. Jørgensen, J.H. Nielsen, S. Hørch, I. Chorkendorff, J.K. Nørskov, Biomimetic Hydrogen Evolution: MoS₂ Nanoparticles as Catalyst for Hydrogen Evolution, *Journal of the American Chemical Society*, 127 (2005) 5308-5309.
- [21] J. Bonde, P.G. Moses, T.F. Jaramillo, J.K. Nørskov, I. Chorkendorff, Hydrogen evolution on nanoparticulate transition metal sulfides, *Faraday Discussions*, 140 (2009) 219-231.
- [22] C. Tsai, K. Chan, F. Abild-Pedersen, J.K. Nørskov, Active edge sites in MoSe₂ and WSe₂ catalysts for the hydrogen evolution reaction: a density functional study, *Physical Chemistry Chemical Physics*, 16 (2014) 13156-13164.
- [23] C. Tsai, K. Chan, J.K. Nørskov, F. Abild-Pedersen, Theoretical insights into the hydrogen evolution activity of layered transition metal dichalcogenides, *Surface Science*, 640 (2015) 133-140.

- [24] T.K. Gajaria, B. Roondhe, S.D. Dabhi, P. Śpiewak, K.J. Kurzydłowski, P.K. Jha, Hydrogen evolution reaction electrocatalysis trends of confined gallium phosphide with substitutional defects, *International Journal of Hydrogen Energy*, 45 (2020) 23928-23936.
- [25] Y. Gao, H. Li, J. Wang, J. Ma, H. Ren, New Insight on Hydrogen Evolution Reaction Activity of MoP₂ from Theoretical Perspective., *Nanomaterials*, 9 (2019) 1270.
- [26] Z. Liang, X. Zhong, T. Li, M. Chen, G. Feng, DFT Study on the Hydrogen Evolution Reaction for Different Facets of Co₂P, *ChemElectroChem*, 6 (2019) 260-267.
- [27] J.A. Libera, J.W. Elam, N.F. Sather, T. Rajh, N.M. Dimitrijevic, Iron(iii)-oxo centers on TiO₂ for visible-light photocatalysis, *Chemistry of Materials*, 22 (2010) 409-413.
- [28] K. Majrik, Z. Pászti, L. Korecz, L. Trif, A. Domján, G. Bonura, C. Cannilla, F. Frusteri, A. Tompos, E. Tálas, Study of PtO_x/TiO₂ Photocatalysts in the Photocatalytic Reforming of Glycerol: The Role of Co-Catalyst Formation., *Materials*, 11 (2018).
- [29] P. Munnik, P.E. de Jongh, K.P. de Jong, Recent Developments in the Synthesis of Supported Catalysts, *Chemical Reviews*, 115 (2015) 6687-6718.
- [30] W. Lamai, A. Bunphung, I. Junumpun, A. Wongkaew, Synthesis and Characterization of Ni@Pt core-shell catalyst over TiO₂ support prepared by incipient wetness impregnation and electroless deposition, *Materials Today: Proceedings*, 17 (2019) 1396-1402.
- [31] Q. Jin, M. Fujishima, H. Tada, Visible-light-active iron oxide-modified anatase titanium(iv) dioxide, *The Journal of Physical Chemistry C*, 115 (2011) 6478-6483.
- [32] S. Rhatigan, E. Sokalu, M. Nolan, G. Colón, Surface Modification of Rutile TiO₂ with Alkaline-Earth Oxide Nanoclusters for Enhanced Oxygen Evolution, *ACS Applied Nano Materials*, 3 (2020) 6017-6033.
- [33] S. Rhatigan, M. Nolan, CO₂ and water activation on ceria nanocluster modified TiO₂ rutile (110), *Journal of Materials Chemistry A*, 6 (2018) 9139-9152.
- [34] M. Fronzi, W. Daly, M. Nolan, Reactivity of metal oxide nanocluster modified rutile and anatase TiO₂: Oxygen vacancy formation and CO₂ interaction, *Applied Catalysis A*, 521 (2016) 240-249.
- [35] H. Tamura, K. Mita, A. Tanaka, M. Ito, Mechanism of Hydroxylation of Metal Oxide Surfaces, *Journal of Colloid and Interface Science*, 243 (2001) 202-207.
- [36] G. Kresse, J. Hafner, *Ab initio* molecular-dynamics simulation of the liquid-metal-amorphous-semiconductor transition in germanium, *Physical Review B*, 49 (1994) 14251-14269.
- [37] J. Furthmüller, J. Hafner, G. Kresse, Dimer reconstruction and electronic surface states on clean and hydrogenated diamond (100) surfaces, *Physical Review B*, 53 (1996) 7334-7351.
- [38] P.E. Blöchl, Projector augmented-wave method, *Physical Review B*, 50 (1994) 17953-17979.
- [39] G. Kresse, D. Joubert, From ultrasoft pseudopotentials to the projector augmented-wave method, *Physical Review B*, 59 (1999) 1758-1775.
- [40] J.P. Perdew, K. Burke, M. Ernzerhof, Generalized gradient approximation made simple, *Physical Review Letters*, 77 (1996) 3865-3868.
- [41] S. Rhatigan, M. Nolan, Activation of Water on MnO_x-Nanocluster-Modified Rutile (110) and Anatase (101) TiO₂ and the Role of Cation Reduction, *Frontiers in Chemistry*, 7 (2019).
- [42] S. Rhatigan, M. Nolan, Impact of surface hydroxylation in MgO-/SnO-nanocluster modified TiO₂ anatase (101) composites on visible light absorption, charge separation and reducibility, *Chinese Chemical Letters*, 29 (2018) 757-764.
- [43] V. Kumaravel, S. Rhatigan, S. Mathew, J. Bartlett, M. Nolan, S.J. Hinder, P.K. Sharma, A. Singh, J.A. Byrne, J. Harrison, S.C. Pillai, Indium-Doped TiO₂ Photocatalysts with High-Temperature Anatase Stability, *The Journal of Physical Chemistry C*, 123 (2019) 21083-21096.
- [44] B.J. Morgan, G.W. Watson, A DFT + U description of oxygen vacancies at the TiO₂ rutile (110) surface, *Surface Science*, 601 (2007) 5034-5041.
- [45] M. Nolan, S.D. Elliott, J.S. Mulley, R.A. Bennett, M. Basham, P. Mulheran, Electronic structure of point defects in controlled self-doping of the TiO₂ (110) surface: Combined photoemission spectroscopy and density functional theory study, *Physical Review B*, 77 (2008) 235424.
- [46] A. Iwaszuk, M. Nolan, Reactivity of sub 1 nm supported clusters: (TiO₂)_n clusters supported on rutile TiO₂ (110), *Physical Chemistry Chemical Physics*, 13 (2011) 4963-4973.

- [47] M. Nolan, Electronic coupling in iron oxide-modified TiO₂ leads to a reduced band gap and charge separation for visible light active photocatalysis, *Physical Chemistry Chemical Physics*, 13 (2011) 18194-18199.
- [48] M. Fronzi, A. Iwaszuk, A. Lucid, M. Nolan, Metal oxide nanocluster-modified TiO₂ as solar activated photocatalyst materials, *Journal of Physics: Condensed Matter*, 28 (2016) 074006.
- [49] M. Fronzi, M. Nolan, Surface Modification of Perfect and Hydroxylated TiO₂ Rutile (110) and Anatase (101) with Chromium Oxide Nanoclusters, *ACS Omega*, 2 (2017) 6795-6808.
- [50] A. Iwaszuk, A.K. Lucid, K.M. Razeeb, M. Nolan, First principles investigation of anion-controlled red shift in light absorption in ZnX (X = O, S, Se) nanocluster modified rutile TiO₂, *Journal of Materials Chemistry A*, 2 (2014) 18796-18805.
- [51] V.I. Anisimov, J. Zaanen, O.K. Andersen, Band theory and Mott insulators: Hubbard U instead of Stoner I, *Physical Review B*, 44 (1991) 943-954.
- [52] S.L. Dudarev, G.A. Botton, S.Y. Savrasov, C.J. Humphreys, A.P. Sutton, Electron-energy-loss spectra and the structural stability of nickel oxide: An LSDA+U study, *Physical Review B*, 57 (1998) 1505-1509.
- [53] C. Byrne, S. Rhatigan, D. Hermosilla, N. Merayo, Á. Blanco, M.C. Michel, S. Hinder, M. Nolan, S. Pillai, Modification of TiO₂ with hBN: High temperature anatase phase stabilisation and photocatalytic degradation of 1,4-dioxane, *Journal of Physics: Materials*, (2019).
- [54] P. Liao, J.A. Keith, E.A. Carter, Water Oxidation on Pure and Doped Hematite (0001) Surfaces: Prediction of Co and Ni as Effective Dopants for Electrocatalysis, *Journal of the American Chemical Society*, 134 (2012) 13296-13309.
- [55] B.A. Baraiya, V. Mankad, P.K. Jha, Adsorption Energetics of Atoms and Diatomic Gases with Electrocatalysis Approach towards Hydrogen and Oxygen Evolution Reaction on Pt Surfaces, *ChemistrySelect*, 3 (2018) 10515-10525.
- [56] J.K. Nørskov, T. Bligaard, A. Logadottir, J.R. Kitchin, J.G. Chen, S. Pandalov, U. Stimming, Trends in the Exchange Current for Hydrogen Evolution, *Journal of The Electrochemical Society*, 152 (2005) J23-J26.
- [57] R. Shannon, Revised effective ionic radii and systematic studies of interatomic distances in halides and chalcogenides, *Acta Crystallographica Section A*, 32 (1976) 751-767.
- [58] A. Walsh, G.W. Watson, Influence of the Anion on Lone Pair Formation in Sn(II) Monochalcogenides: A DFT Study, *The Journal of Physical Chemistry B*, 109 (2005) 18868-18875.
- [59] A. Iwaszuk, M. Nolan, SnO-nanocluster modified anatase TiO₂ photocatalyst: exploiting the Sn(ii) lone pair for a new photocatalyst material with visible light absorption and charge carrier separation, *Journal of Materials Chemistry A*, 1 (2013) 6670-6677.
- [60] J.C. Ortiz-Rodríguez, N.R. Singstock, J.T. Perryman, F.P. Hyler, S.J. Jones, A.M. Holder, C.B. Musgrave, J.M. Velázquez, Stabilizing Hydrogen Adsorption through Theory-Guided Chalcogen Substitution in Chevrel-Phase Mo₆X₈ (X=S, Se, Te) Electrocatalysts, *ACS Applied Materials & Interfaces*, 12 (2020) 35995-36003.
- [61] A.L. Allred, Electronegativity values from thermochemical data, *Journal of Inorganic and Nuclear Chemistry*, 17 (1961) 215-221.

M4X4-modified-TiO2-HER-text.pdf (1.31 MiB)

[view on ChemRxiv](#) • [download file](#)

Modification of TiO₂ with Metal Chalcogenide Nanoclusters for Hydrogen Evolution

Stephen Rhatigan¹, Lorenzo Niemitz¹ and Michael Nolan*^{1,2}

1: Tyndall National Institute, UCC, Lee Maltings, Dyke Parade, Cork, T12 R5CP, Ireland

2: NIBEC, Ulster University, Shore Road, Co Antrim, BT37 OQB, Northern Ireland

[*Michael.nolan@tyndall.ie](mailto:Michael.nolan@tyndall.ie)

Supplementary Material

This document contains supplementary material relevant to the paper entitled: “*Modification of TiO₂ with Metal Chalcogenide Nanoclusters for Hydrogen Evolution*”.

List of Figures:

- S1: Relaxed atomic structures of M₄X₄ nanoclusters (M = Sn, Zn; X = S, Se).
- S2: Schematic diagram of the relationship between the energies computed in the photoexcited model.
- S3: Adsorption configurations of H adsorbed at Sn₄Se₄-r110 for coverages from 1-6 H.
- S4: Adsorption configurations of H adsorbed at Zn₄S₄-r110 for coverages from 1-6 H.
- S5: Adsorption configurations of H adsorbed at Zn₄Se₄-r110 for coverages from 1-6 H.

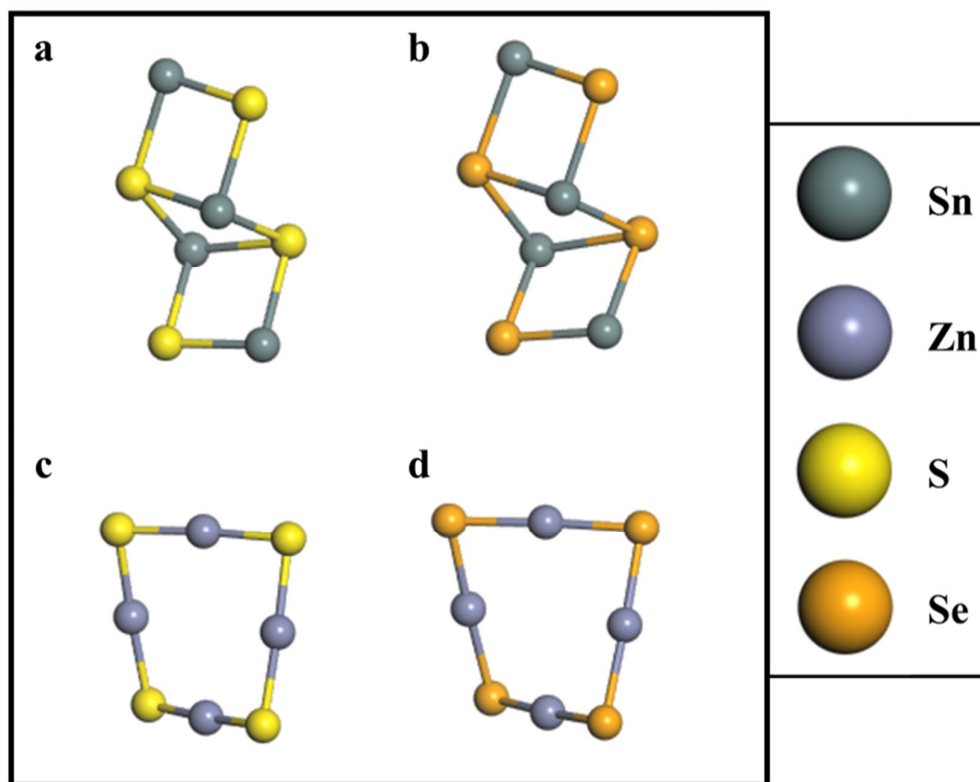


Figure S1 Relaxed atomic structures of (a) Sn_4S_4 , (b) Sn_4Se_4 , (c) Zn_4S_4 and (d) Zn_4Se_4 .

Photoexcitation is modelled by imposing a triplet electronic state on the system to promote an electron to the conduction band, with a corresponding hole in the valence band. This model examines the energetics and charge localization associated with photoexcitation. The following energies are computed:

- The ground state energy of the system, yielding $E^{singlet}$.
- A single point energy calculation of the triplet electronic state at the ground state geometry, which gives $E^{unrelaxed}$.
- The fully relaxed triplet electronic state which gives $E^{relaxed}$.

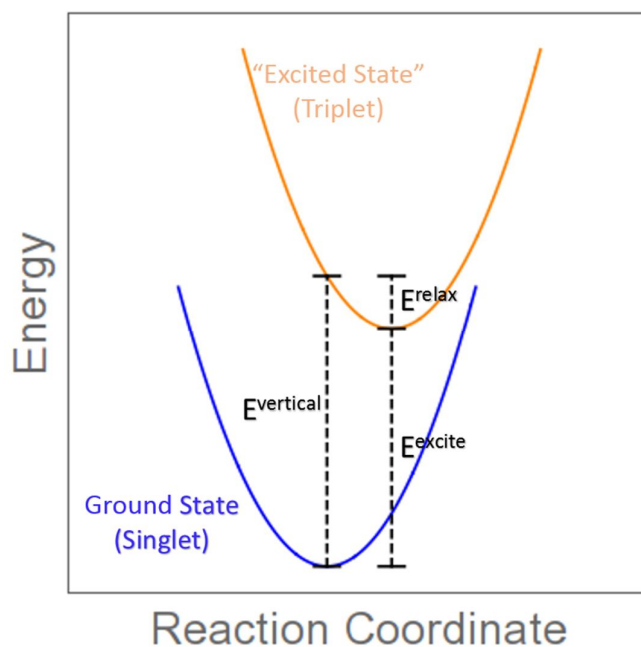


Figure S2 Schematic diagram of the relationship between the energies computed in the photoexcited model.

From the results of these calculations we compute:

1. The singlet-triplet vertical excitation energy:

$$E^{vertical} = E^{unrelaxed} - E^{singlet}.$$

This is the difference in energy between the ground (singlet) state and the imposed triplet state at the singlet geometry and corresponds to the simple VB-CB energy gap from the computed density of states.

2. The singlet-triplet excitation energy:

$$E^{excite} = E^{relaxed} - E^{singlet}.$$

This is the difference in energy between the relaxed triplet state and the relaxed singlet state and gives a crude approximation of the excitation energy.

3. The triplet relaxation (carrier trapping) energy:

$$E^{relax} = E^{unrelaxed} - E^{relaxed}.$$

This difference in energy between the unrelaxed and relaxed triplet states is the energy gained when the electron and hole are trapped at their metal and oxygen sites upon structural relaxation. This energy relates to the stability of the trapped electron and hole.

These quantities are summarized schematically in **Figure S2**.

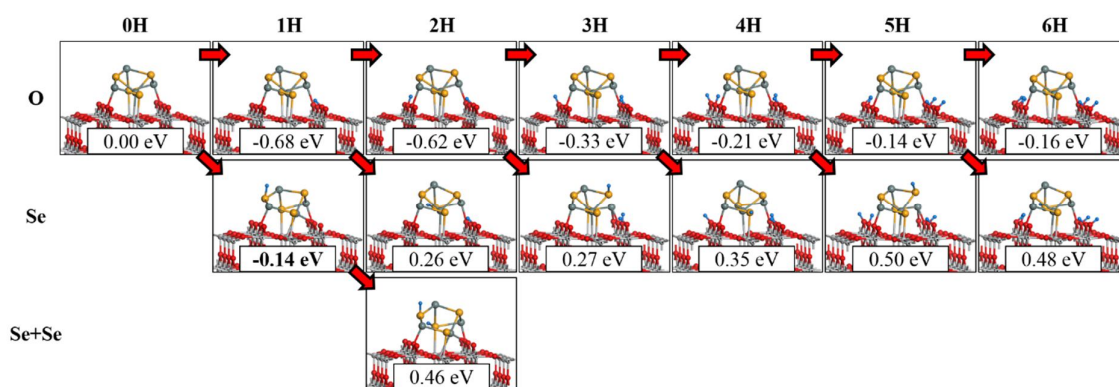


Figure S3 Adsorption configurations of H adsorbed at $\text{Sn}_4\text{Se}_4\text{-r110}$ for coverages between one and six H atoms. The top row shows H adsorbed only at surface (O_{br}) sites, the second row shows configurations in which 1 H is adsorbed at a cluster (Se) site, at each coverage. The configuration in the third row has 2 H adsorbed at Se sites. The adsorption free energies, ΔG_{H} , are included in the insets and the red arrows indicate the configurations relative to which ΔG_{H} is computed. At all coverages, H adsorption at O_{br} sites is more favourable than adsorption at cluster sites.

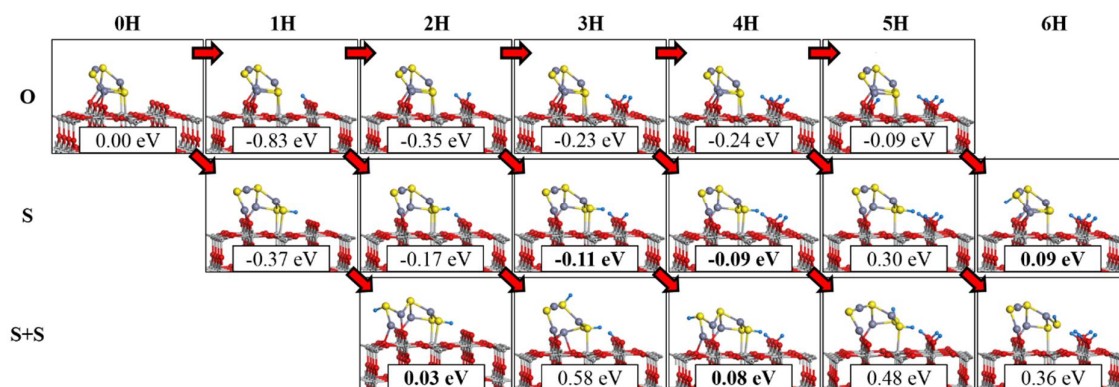


Figure S4 Adsorption configurations of H adsorbed at $\text{Zn}_4\text{S}_4\text{-r110}$ for coverages between one and six H atoms. The top row shows H adsorbed only at surface (O_{br}) sites, the second row shows configurations in which 1 H is adsorbed at a cluster (S) site, at each coverage. The configurations in the third row have 2 H adsorbed at S sites, for each coverage. The adsorption free energies, ΔG_{H} , are included in the insets and the red arrows indicate the configurations relative to which ΔG_{H} is computed. At all coverages, H adsorption at O_{br} sites is more favourable than adsorption at cluster sites.

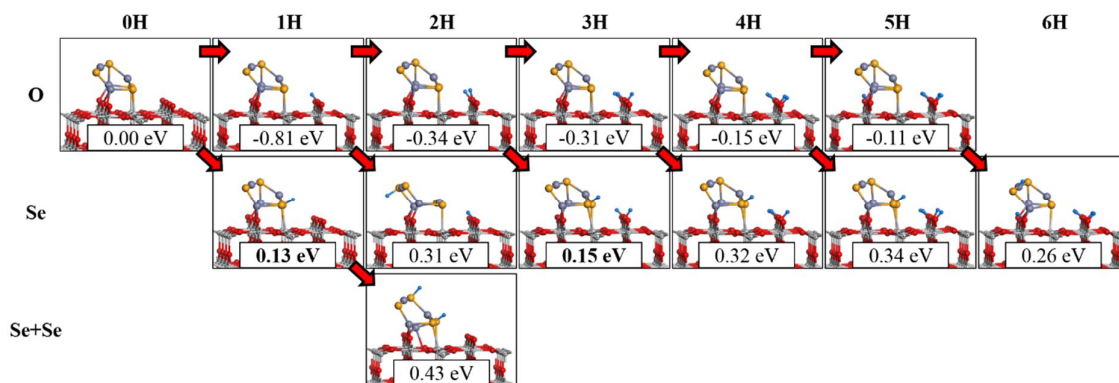


Figure S5 Adsorption configurations of H adsorbed at $\text{Zn}_4\text{Se}_4\text{-r110}$ for coverages between one and six H atoms. The top row shows H adsorbed only at surface (O_{br}) sites, the second row shows configurations in which 1 H is adsorbed at a cluster (Se) site, at each coverage. The configuration in the third row has 2 H adsorbed at Se sites. The adsorption free energies, ΔG_{H} , are included in the insets and the red arrows indicate the configurations relative to which ΔG_{H} is computed. At all coverages, H adsorption at O_{br} sites is more favourable than adsorption at cluster sites.

SuppInfo.pdf (709.77 KiB)

[view on ChemRxiv](#) • [download file](#)
